On the Determination of K_V in the Near-Surface Ocean from Acoustic Measurements of Bubbles

S. A. THORPE

Institute of Oceanographic Sciences, Wormley, Godalming, Surrey, GU8 5UB, U.K.

(Manuscript received 17 October 1983, in final form 9 January 1984)

ABSTRACT

When wind waves break in deep water, clouds of small bubbles are produced which are diffused downwards by turbulence. We describe here how the vertical diffusion coefficient K_v of the turbulence near the sea surface may be determined from measurements of the bubbles made using a subsurface, upward-directed, high-frequency sonar. The method consists of comparing the observed distributions of scattering cross section with those which can be predicted. Existing observations are used to demonstrate the use of the technique, but are not yet sufficient to allow precise determination of K_v or of its variation with depth or wind speed.

1. Introduction

It is usually extremely difficult to make precise direct measurements of any useful physical quantity just below the sea surface because of the violence of water motions and the orbital velocities induced by waves. Apart from the difficulties of maintaining surface-following moorings or of recovering profiling instruments in rough weather, the *in situ* instruments themselves, or perhaps the towing or launch-and-recovery vessels, are often prone to disturb (or are suspected of disturbing) the very quantities the observer wishes to measure. Freely floating instruments may tend to move into regions of convergence, in particular into wind rows, and may not sample the water in an unbiased manner. In consequence, knowledge of the dynamics of the upper ocean boundary layer is meagre in comparison with that of the atmospheric boundary layer over land, or even of the ocean's benthic boundary layer, inspite of its being one of the most extensive and important of the fluid boundary layers on our planet.

There is some merit in examining alternative, less direct, methods of observation. We discuss here the possibility of estimating the vertical turbulent diffusion coefficient (K_v) from remote sonar measurements of subsurface bubbles created by breaking wind waves. The distribution of bubbles below the surface is established primarily by turbulence, and hence from knowledge of the distribution it should, in principle at least, be possible to infer information about the turbulence. The method relies on the detection of bubbles from a moored or bottom mounted, upward-directed, narrow-beam, sonar suitably calibrated to produce outputs *proportional to* (but not necessarily equal to) the acoustic scattering cross-section per unit volume (M_v) (units m^{-1}), of the bubbles at several depths below the surface.

2. The method

We shall assume that the turbulent diffusion coefficient for bubbles is equal to that of momentum. Observational evidence to support this assumption is lacking, although it appears valid in sediment flow (Newberger and Caldwell, 1981) which has similar physics, and is a common assumption in other related situations (e.g., in radiation fog; see Brown, 1980). It is worth noting that a description of turbulence by means of eddy diffusion coefficients is often inappropriate or, at best, dubious. It is however in steady, or quasi steady, boundary layers that they can be used with greatest confidence and success (see Pasquill, 1974). Analytical results derived from studies of the atmospheric boundary layer by Hunt and Weber (1979) suggest that the use of a diffusion equation to represent turbulent diffusion from ground-level sources is justifiable.

The method was hinted at in an earlier paper (Thorpe, 1982, hereafter referred to as I) in which the interested reader may find more extensive discussion of the sonar observations. The principle is perhaps best illustrated by resort to solutions of a simple equation representing the bubbles. We suppose that the subsurface distribution of bubbles results from:

1) turbulent transport from a source (or sources—the whitecaps) at the surface. The turbulence in the near-surface layer includes turbulence generated by the breaking waves as well as that induced by shear, breaking internal waves, Langmuir circulation, and so on;

2) the buoyant rise of bubbles; and
3) the change in the radius of bubbles due to i) the diffusion of gases from the bubbles into the water and ii) compression of bubbles under hydrostatic pressure.

In a steady state the simplest equation representing a balance of these processes is

$$\frac{d}{dz}\left(K_v \frac{dN}{dz}\right) + w_b \frac{dN}{dz} - \sigma N = 0, \tag{1}$$

where N represents the number of bubbles per unit volume at depth z and tends to zero as z tends to infinity, w_b is the bubbles' rise speed and σ represents the processes involved in 3) above. We shall imagine that the bubbles have all about the same radius a_0. (This is not implausible. Large bubbles rise rapidly to the surface and are thus not plentiful, while very small bubbles dissolve rapidly. The size distribution is thus narrow with a pronounced peak; see Johnson and Cooke, 1979). Since w_b depends only on radius and not on z (see I), we suppose w_b = constant. The processes 3) of course involve a change in bubble radius, and the term $-\sigma N$ is chosen for simplicity to characterize a term representing a loss of bubbles from the population N by collapse. The objective here is to illustrate the processes rather than to describe them in detail. Their complexity is more fully accounted for in Section 4.

If we suppose (model A) that K_v and σ are independent of depth, then the solution of (1) is

$$N = N_0 \exp(-\beta z), \tag{2}$$

where N_0 is a constant determined here (and in later models) by a surface boundary condition, and

$$K_v\beta^2 - w_b\beta - \sigma = 0. \tag{3}$$

If, therefore, we can determine

$$\beta = -\frac{1}{N}\frac{dN}{dz} = -\frac{d}{dz}(\ln N) = d^{-1}, \tag{4}$$

say, by observations, and if σ and w_b are known or can be estimated then, from (3)

$$K_v = w_b d + \sigma d^2 \tag{5}$$

may be found.

In I it was shown that M_v is approximately equal to the area of the bubbles per unit volume, provided that a sonar of sufficiently high frequency is used, namely one such that the peak in the size distribution lies well above the resonant radius, so that the power scattered from resonant bubbles is small compared to the total scattered power. Thus *in our simple model*, $M_v = 4\pi a_0^2 N$ and

$$d^{-1} = -\frac{d}{dz}(\ln M_v), \tag{6}$$

so d, and hence K_v (using 5), may be determined from the sonar measurements.

This is the essence of the inverse method. It is of great advantage that the determination of d in (6) does not depend on the accurate measurement of M_v which, for reasons associated with sonar calibration, is very difficult to achieve. It is only necessary to obtain a measure proportional to M_v.

3. Further analytical solutions

To illustrate the method in more generality, we may solve (1) for K_v. Writing

$$\theta = -\frac{1}{N}\frac{dN}{dz} \tag{7}$$

in (1) we have

$$\frac{dK_v}{dz} + K_v\left(\frac{1}{\theta}\frac{d\theta}{dz} - \theta\right) = -\left(w_b + \frac{\sigma}{\theta}\right), \tag{8}$$

which we now regard as an equation for the (unknown) K_v in terms of the (known) θ. Using the integrating factor $\theta \exp(-\int \theta dz)$ we may integrate (8) to obtain

$$K_v(z) = f(z)\left[K_v(z_0)\theta(z_0) - \int_{z_0}^{z}\left(\frac{\sigma + \theta(y)w_b}{f(y)}\right)dy\right], \tag{9}$$

where $f(z) = \theta^{-1}\exp[\int_{z_0}^{z}\theta(y)dy]$ and z_0 is some level at which K_v is known (e.g., zero at great depth), or via which we select $K_v(z_0)$ so that the form is bounded or everywhere positive. However while it is thus, in principle, possible to compute K_v from the measured $\theta(z)$, it is simpler in practice to assume some definite form for K_v as we did in model A, and to compare the observed profiles of N (or M_v) with those determined by the solution of (1). We have examined three other models. (A summary of the main features of the models is given in Table 1):

Model B: $K_v = ku_*z$, σ = constant.

This form of K_v is that appropriate to constant stress layer in the atmospheric or benthic boundary layer. There is also evidence to support a coefficient of this form in the upper ocean boundary layer (Dillon *et al.*, 1981) although not from observations very close to the surface. Information there is lacking. The solution of (1) is

$$N = N_0 z^{-\lambda/2}\mathcal{K}_\lambda(y), \tag{10}$$

where $y = (4\sigma z/ku_*)^{1/2}$, $\lambda = w_b/ku_*$, and $\mathcal{K}_\lambda$ is the modified Bessel Function;

$$\theta = \frac{\lambda}{2z} - \left(\frac{\sigma}{ku_*z}\right)^{1/2}\frac{\mathcal{K}'_\lambda}{\mathcal{K}_\lambda}. \tag{11}$$

Model C. K_v independent of z, $\sigma = \alpha z$.

Here we revert to the form of K_v chosen in model A, but allow σ to adopt a more realistic form (see I, Section 4.3.1). The solution is

$$N = N_0 \exp\left(-\frac{w_b z}{2K_v}\right)A_i(y), \tag{12}$$

where

$$y = \left(\frac{K_v}{\alpha}\right)^{2/3}\left(\frac{\alpha z}{K_v} + \frac{w_b^2}{4K_v^2}\right),$$

and A_i is the Airy Function;

$$\theta = \frac{w_b}{2K_v} - \left(\frac{\alpha}{K_v}\right)^{1/3}\frac{A_i'}{A_i}. \tag{13}$$

Model D. $K_v = ku_*z$, $\sigma = \alpha z$.

The solution was given in I (except for a misprint);

$$N = N_0 y^{-\lambda/2}\mathcal{H}_{\lambda/2}(y), \tag{14}$$

where $y = (\alpha/ku_*)^{1/2}z$ (selected curves are shown in I, figure 25);

$$\theta = \frac{\lambda}{2z} - \left(\frac{\alpha}{ku_*}\right)^{1/2}\frac{\mathcal{H}'_{\lambda/2}}{\mathcal{H}_{\lambda/2}}. \tag{15}$$

The solutions have been used to plot ln$N$ versus z for models A and B (Fig. 1) and $d(z)$ as a function of the local value of k_v at 2 m and 4 m depth (Fig. 2). We have selected w_b = 0.54 cm s^{-1}, the rise speed of bubbles of radius 50 μm at the peak in the size distribution observed by Johnson and Cooke, and σ = 0.018 s^{-1} for models A and B, a value which gives a bubble lifetime of about 1 min (corresponding to observations; see Thorpe and Hall, 1983) and which we shall show later is consistent with other more complex, but more realistic, models. The value of α in models C and D is taken so that σ = 0.018 s^{-1} at 2 m or 4 m. The close correspondence of points from the different models indicates that the determination of the local value of K_v from the estimated θ is not very sensitive to the overall profile of K_v (or σ) which is chosen, provided perhaps that it does not change too rapidly.

An indication of the effect of curvature in the K_v profile is given in a solution derived from a parametric representation of (8):

$$K_v = \frac{R(w_b + R)}{\sigma + R'}, \quad \theta = \frac{\sigma + R'}{R}, \tag{16}$$

where R is the parameter, a function of z. Choosing $R = A + Bz$ leads to K_v having a quadratic form in z which can be written

$$K_v = w_b d + (\sigma + B)d^2, \tag{17}$$

a form similar to (5) but now having the additional term Bd^2. This curve will thus differ from (5), or the points plotted in Fig. 2 for models A–D, when B becomes comparable to σ, or when

$$\frac{d^2K_v}{dz^2} \sim \sigma.$$

Points corresponding to $B = 0.5\sigma$ are shown in Fig. 2a and fall progressively further below those of the earlier models.

Subject to the sweeping range of assumptions made so far, the results shown in Fig. 2 suggest that K_v might be determined from *local* estimates of d to an accuracy, independent of the model, of perhaps 25%, provided d is within the range considered. However, by observing the form of the profile of ln$N$ as shown in Fig. 1, or equivalently of lnM_v, and by forming estimates of K_v at different depths and in different wind speeds, it may be possible to decide whether the calculated profiles of K_v are consistent with the adopted model.

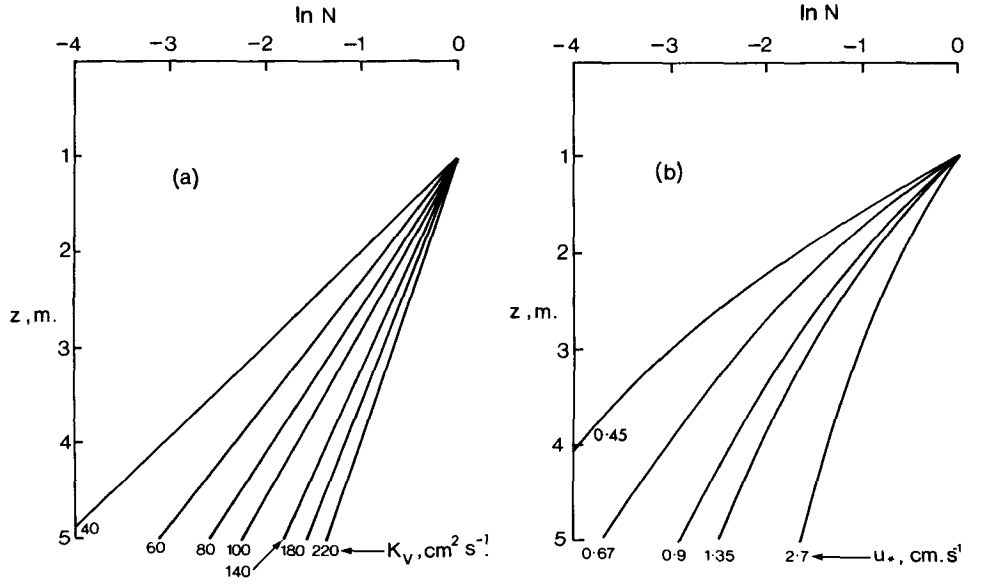

FIG. 1. Profiles of ln$N$, normalized to unity at 1 m, vs. depth (z) for various values of (a) K_v, independent of depth (model A), and (b) u_*, where $K_v = ku_*z$, with k = 0.4 (model B); w_b = 0.54 cm s^{-1} and σ = 0.018 s^{-1}.

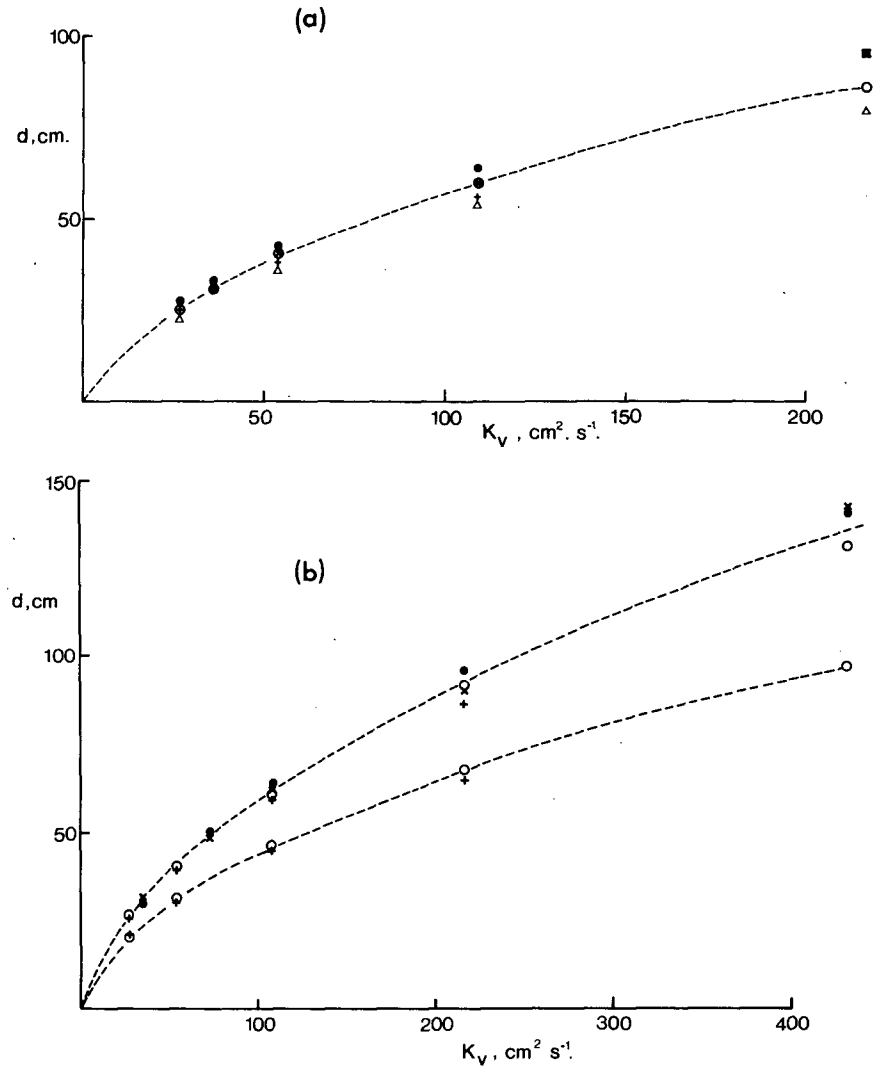

FIG. 2. Variation of d with K_v at (a) 2 m and (b) 4 m. The points are (closed circles) model A; (crosses) model B; (open circles) model C; (plus signs) model D; and, in (a) (triangle) $K_v = w_b d + 1.5\sigma d^2$ (see text); $w_b = 0.54$ cm s^{-1}. In (a) $\sigma = 0.018$ s^{-1} or $\alpha = 4.5 \times 10^{-5}$ cm^{-1} s^{-1} so that $\alpha z = \sigma$. The upper set of points in (b) have $\sigma = 0.018$ s^{-1} or $\alpha = 9 \times 10^{-5}$ cm^{-1} s^{-1}, so that $\alpha z = \sigma$, while the lower set have $\alpha = 4.5 \times 10^{-5}$ cm^{-1} s^{-1} as in (a).

4. Numerical models

Two different types of numerical models have been devised to describe the dispersion of bubble clouds containing a broad range of bubble sizes. In principle they are similar to the analytical models in that they include the three processes represented in (1) and assume that a steady state is reached. Now, however, the effect of change in bubble radius is more accurately accounted for, either i) by allowing a flux in radius space from one bubble size to another in a differential equation for the number of bubbles of a given radius per unit volume, or ii) by following the changes which occur in a single bubble during its lifetime.

Model (i) is described in I (Section 4.3.2.). The first two terms in the differential equation are exactly as in (1). The term σN is however replaced by

$$\chi \equiv \frac{\partial}{\partial a}\left(\frac{da}{dt}\right)N + \frac{da}{dt}\frac{\partial N}{\partial a}, \tag{18}$$

where a is the bubble radius and da/dt represents the rate changes due to gas flux and change in hydrostatic pressure. The equation is solved with a given distribution of bubbles $N = N_0(a)$ for $a < a_{max}$ at a shallow depth $z = z_0$, and with $N = 0$ at $a \geq a_{max}$ and at $z = z_1$, a large depth. Solutions appear to be fairly insensitive to the form of $N_0(a)$ (see I).

Turbulence in model (ii) is simulated by a Monte-Carlo, or random walk, technique (Thorpe, 1984a) in which individual particles, representing bubbles, move at each time step Δt through a distance

$$\Delta z = (v - w_b)\Delta t,$$

where $v = v_0 \cos\phi$, ϕ is a random angle between 0 and 2π radians, and v_0 is a prescribed velocity. The effective K_v is constant with depth and is equal to $v_0^2\Delta t/4$ (see Csanady, 1973). During the period Δt the bubble radius changes by an amount $\Delta t da/dt$. Particles with a range of different sizes are continually fed in at level $z = 0$ (the surface). Those subsequently reaching this level are lost. The integration is continued until a steady state is reached. The solutions are again fairly insensitive to the distribution of bubble sizes at the surface. This model should provide a more accurate representation of flux in radius space than does the diffusion equation, and is particularly valuable when the bubbles are composed of more than one gas.

Both models depend on a number of important assumptions, for example about the nature of the surface of the bubbles, particularly its effect on gas transfer and surface tension. They neglect coalescence of bubbles and the effect of turbulence on gas flux. They assume that a steady state is maintained and that the source can be represented by a uniform distribution. These assumptions are discussed in I and in Thorpe (1984b). They appear to be valid only when the wind speed is in a limited range, greater than 6 m s^{-1} and less than 20 m s^{-1}, but more data is needed to confirm this. They are violated in the breaking waves themselves and so may not be valid very close to the sea surface.

From the models we have calculated the vertical distributions of $\ln M_v$ for a sonar of the frequency used in the observations, 248 KHz. These distributions are shown in Fig. 3. To produce them we had to adopt certain forms for w_b and da/dt and to select values of diffusion coefficients, surface tension, viscosity, acceleration due to gravity, and the adsorption coefficients, and these are all explained in I (Sections 3.1–3.3). In model (i) we have used K_v independent of depth [Fig. 3a; we refer to this model as (ia)] and equal to ku_*z (Fig. 3b; model (ib). See Table 1 for guidance). The results of model (ii) are shown in Fig. 3c. Comparison of Figs. 3a and 3c shows that there is reasonable agreement between the two models in the shape of the curves. The effect of modeling the bubble size distribution in a more realistic way when K_v is independent of depth, is seen by comparing these figures with Fig. 1a. The values of $\ln M_v$, proportional to $\ln N$ in Fig. 1, are progressively reduced as depth increases. A similar trend is found for $K_v = ku_*z$ when Figs. 3b and 1b are compared. (It may also be seen by comparing Fig. 1b with the more realistic representation of σ in model D plotted in I, Fig. 25.) The numerical models show that M_v decays more nearly exponentially when $K_v = ku_*z$ than when K_v is independent of depth, in contrast to the analytical results of models A and B.

The variation of $d(6)$ with K_v at 2 m and 4 m is shown in Fig. 4. As in Fig. 2, the models agree surprisingly well. The similarity between the curves in Figs. 2a and 4a results from our choosing σ so that the values of d from model A and from model (ia) were in best agreement at $z = 1.5$ m for $40 \leqslant K_v$ (cm^2 s^{-1}) $\leqslant 180$. The effect of varying the saturation level of the gases in the water by ±3% is also shown in Figs. 3 and 4. The value of d increases by about 3% for an increase of 1% in saturation level. The effect of a change in temperature of 1 K produces, through its effect on viscosity, diffusivity, and adsorption coefficients, a 5% change in d. Changes in the stability of the air–sea boundary measured by the value of L, the Monin-Obukov length, may also be accounted for by using model (i) with appropriate choice of K_v (see Fig. 4).

5. Observations

Measurements with a vertically pointing sonar were made at a coastal site near Oban in NW Scotland and in the fresh-water Loch Ness. Fig. 5 shows the variation of $\ln M_v$ with depth at Oban at various wind speeds. The slope of the lines drawn through the points increases with wind speed, and the decay of M_v with depth is approximately exponential. Similar trends were found in Loch Ness although with generally lower values of M_v. Johnson and Cooke's (1979) data based on photographic observations of bubbles have been used to calculate M_v and these values are also shown in Fig. 5. They agree well with the sonar data.

The linear trend of points in Fig. 5 suggest that of the two vertical distributions of K_v considered in Section 4, $K_v = ku_*z$ should most nearly represent the data. We have therefore, in Fig. 6, plotted the value of d estimated at 2 m against K_v at the same depth, determining u_* from the wind speed by assuming that the stress is continuous: $u_* = (C_D r)^{1/2} W_{10}$, where W_{10} is the wind speed at 10 m, C_D the drag coefficient

TABLE 1. Summary of models.

Model	K_v (I = independent of depth)	Terms representing change in bubbles' radius	Type of model
A	I	σN; σ independent of depth	Analytical, diffusion equation
B	ku_*z	σN; σ independent of depth	Analytical, diffusion equation
C	I	σN; $\sigma \propto z$	Analytical, diffusion equation
D	ku_*z	σN; $\sigma \propto z$	Analytical, diffusion equation
(ia)	I	x [Eq. (18)]	Numerical, diffusion equation
(ib)	ku_*z	x [Eq. (18)]	Numerical, diffusion equation
(ii)	I	see Thorpe (A)	Numerical, random walk

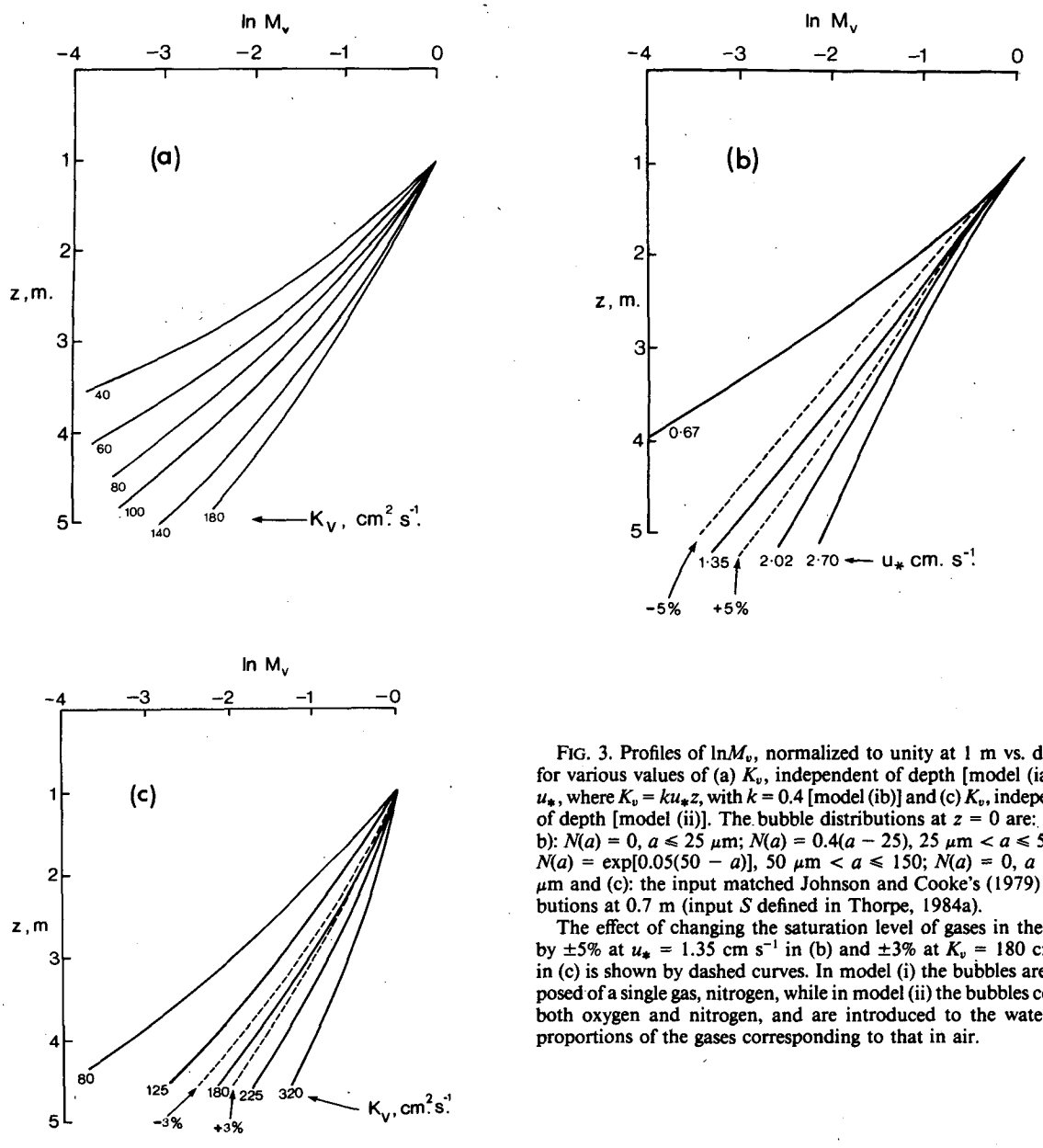

FIG. 3. Profiles of $\ln M_v$, normalized to unity at 1 m vs. depth z for various values of (a) K_v, independent of depth [model (ia)], (b) u_*, where $K_v = ku_*z$, with $k = 0.4$ [model (ib)] and (c) K_v, independent of depth [model (ii)]. The bubble distributions at $z = 0$ are: (a and b): $N(a) = 0$, $a \leqslant 25$ μm; $N(a) = 0.4(a - 25)$, 25 μm $< a \leqslant 50$ μm; $N(a) = \exp[0.05(50 - a)]$, 50 μm $< a \leqslant 150$; $N(a) = 0$, $a \geqslant 150$ μm and (c): the input matched Johnson and Cooke's (1979) distributions at 0.7 m (input S defined in Thorpe, 1984a).

The effect of changing the saturation level of gases in the water by ±5% at $u_* = 1.35$ cm s^{-1} in (b) and ±3% at $K_v = 180$ cm^2 s^{-1} in (c) is shown by dashed curves. In model (i) the bubbles are composed of a single gas, nitrogen, while in model (ii) the bubbles contain both oxygen and nitrogen, and are introduced to the water with proportions of the gases corresponding to that in air.

(taken as 1.3×10^{-3}) and r is the ratio of the density of air to that of water. The solid line shows the results of the calculations using model (ia). The bubble size distributions at the surface remain similar as wind speed increases. No adjustment of parameters has been made except that neutral stability is assumed ($L^{-1} = 0$ m^{-1}). This was probably a reasonable average of the conditions. There is fair agreement between the model and the observations up to values of K_v of about 100 cm^2 s^{-1}, $W_{10} = 10$ m s^{-1}, particularly if we allow for a probable supersaturation which would lift the theoretical curve. Higher values of K_v than found using ku_*z are needed to explain the large values of d at higher wind speeds. These values cannot be accounted for by an increase in saturation levels due to gas transfer into the water from the bubbles themselves (see Thorpe, 1984c). If only a fraction of the wind stress is transferred to the water (see Donelan, 1978) the points in Fig. 6 shift to lower values of K_v and diverge further from the theoretical curve.

Although the models with uniform K_v are less likely to be appropriate, we have plotted estimates of K_v at 1.5 m in Fig. 7, supposing now that model (ia) is valid and finding K_v from the values of d from Fig. 5 and

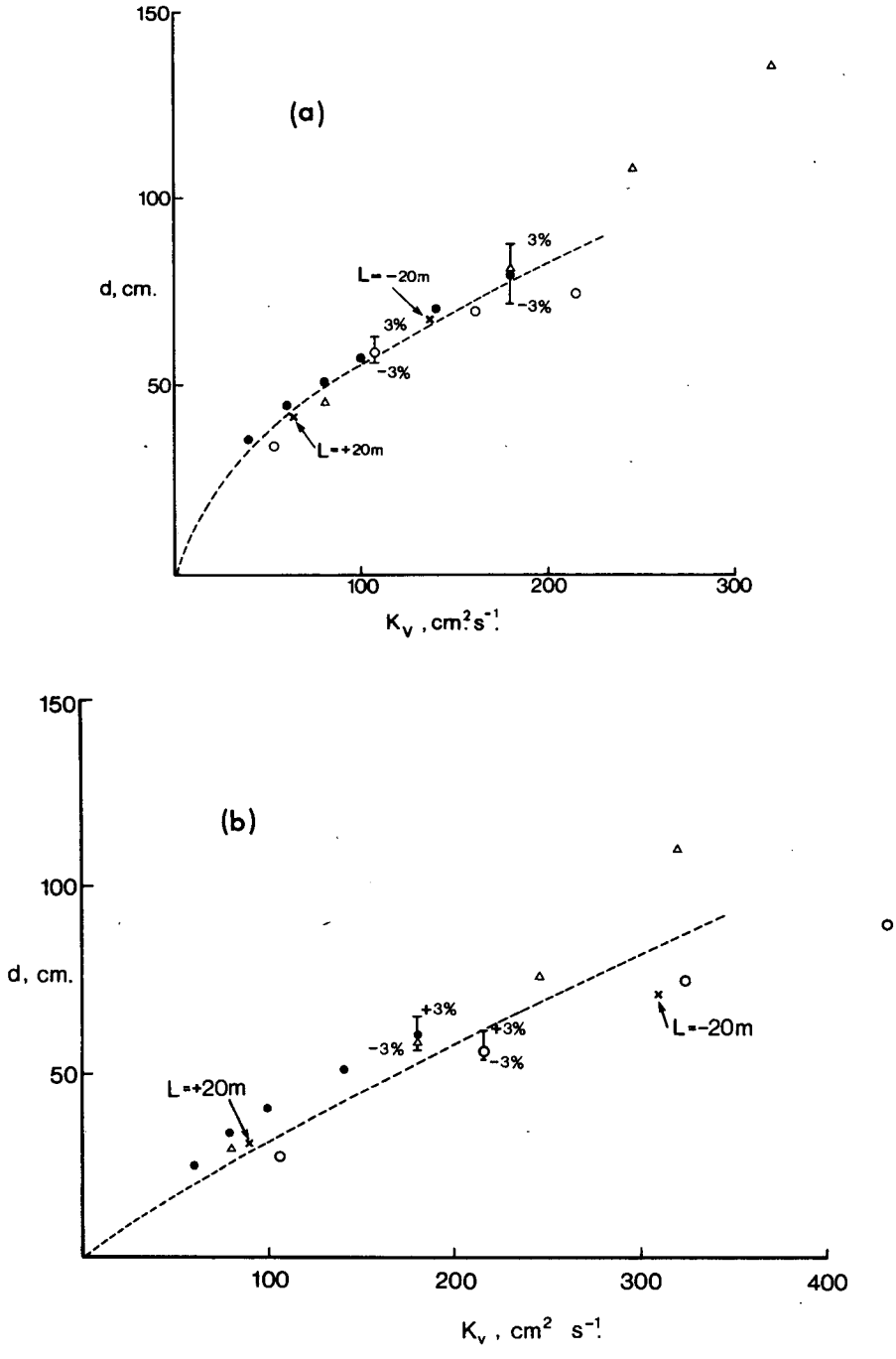

FIG. 4. Variation of d with K_v at (a) 2 m and (b) 4 m. The points are (solid circles) model (ia); (open circles) model (ib); (triangles) model (ii). The points x are for model (i) with $K_v = ku_* z\phi_m^{-1}$, where $\phi_m = 1 + 7z/L$ in stable conditions ($L > 0$) and $(1 - 16z/L)^{-1/4}$ in unstable conditions ($L < 0$), evaluated at $u_* = 1.35$ cm s^{-1} and $L = \pm 20$ m.

the model points in Fig. 4a. There is considerable scatter, but a clear increase with wind speed.

6. Discussion

The data are not yet sufficient to draw definite and useful conclusions about the variation of K_v with depth and wind speed. There is too much scatter in the points of Fig. 5; the curve shapes are uncertain. The general increase in d with wind speed appears however to be a decided trend, and thus, whatever selection is made amongst the models considered, K_v appears to increase with wind. This is no surprise. The present evidence

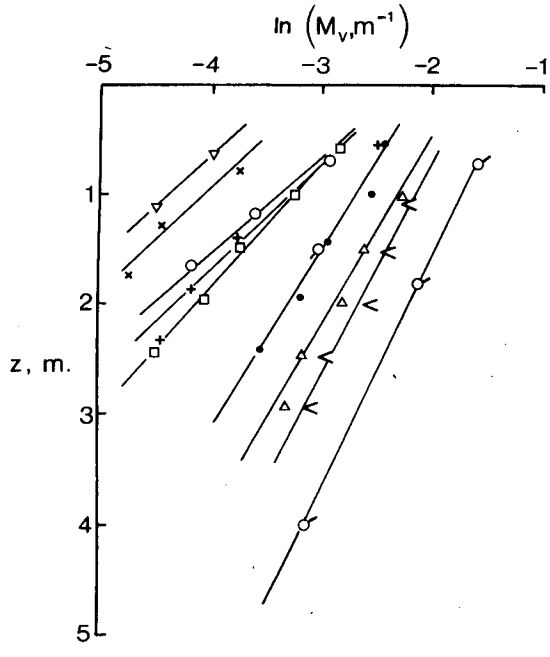

FIG. 5. The variation of $\ln M_v$ with depth at various wind speeds: (inverted triangles) 3.25 m s^{-1}; (crosses) 4.75 m s^{-1}; (open circles) 5.99 m s^{-1}; (plus signs) 7.52 m s^{-1}; (squares) 8.42 m s^{-1}; (solid circles) 9.41 m s^{-1}; (triangles) 10.42 m s^{-1}; (left angle brackets) 11.51 m s^{-1}; The points and are from Johnson and Cooke's (1979) measurements at 8–10 and 11–13 m s^{-1} winds respectively.

favors a distribution $K_v = ku_*z$, at least up to winds of about 10 m s^{-1} at depths of 2 m, but does not provide substantial confirmation.

It is tempting to suggest that the deviation of points from the curve in Fig. 6 is the result of the enhanced

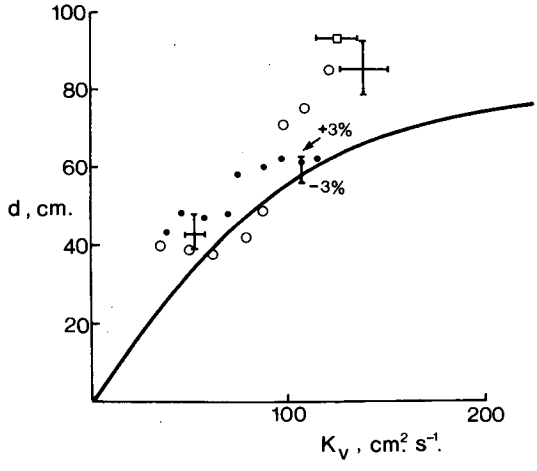

FIG. 6. The variation of d, found from Fig. 5, with K_v at 2 m depth. The values of $K_v = ku_*z$ are determined from the wind speed. The solid line is from the results of model (ib) shown in Fig. 4a. The points are from Oban (open circles), from Loch Ness (solid circles), and Johnson and Cooke (1979) (squares). The crosses represent error estimates in the data and the vertical bar shows effect of changing the saturation level by ±3%.

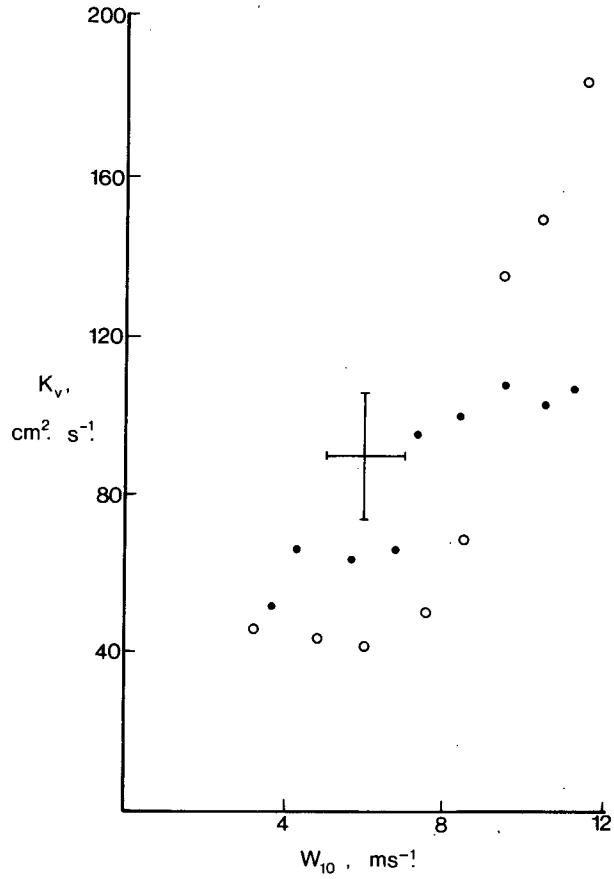

FIG. 7. The variation of K_v at 1.5 m depth with W_{10}, supposing that model (ia) is valid. The points are: from Oban (open circles) and from Loch Ness (solid circles). The cross represents the error estimates of the data.

importance of turbulence caused by breaking waves as wind increases. What new scaling might this involve? The friction velocity in the air w_* the acceleration due to gravity g and the fetch x are all likely to be important. Other possible dimensional parameters such as surface tension and viscosity, significant in bubble dynamics and in capillary waves, are probably less important unless they are responsible for establishing roughness and velocity scales during the break-up of large trapped bubbles in spilling or plunging whitecaps. The rms wave amplitude ζ is only a secondary variable, being dependent itself on g, x and w_* (Phillips, 1977), but a scaling like that of ζ appears a possible candidate for the depth, d_*, at which breaking wave-generated turbulence becomes comparable to that generated by shear. If so, assuming neutral stability, it follows that

$$d_* = c\left(\frac{w_*^2 x}{g}\right)^{1/2},$$

The present data, at approximately $x = 10$ km, would suggest that $c = 0.17$, and $d_*/\zeta = 14$. This, if correct, is surprisingly large. The form of K_v in $0 < z < d_*$ must be regarded as unknown.

Work is in hand to extend the sonar observations to a site remote from shore.

Since this work was accepted for publication I have seen the paper by Kitaigorodski *et al.* (1983) who report direct measurements of turbulence using a drag sphere. They picture "a two layer structure; the upper layer, with thickness 10ζ, is a region of intense turbulence generation by waves, while below this region the more classical notion of a constant stress layer is appropriate."

The similarity of their conclusions to our own, following from totally different means of observation, is heartening and gives confidence in the value of the acoustic, remote sensing, technique.

Acknowledgment. This was written during a visit to the School of Oceanography, Oregon State University, Corvallis, in summer 1983, and I wish to express my gratitude to my hosts, particularly Doug Caldwell and Tom Dillon for arranging the visit and providing such poor weather that I was not distracted by outdoor leisure activities during the first half of my stay. Partial support was received from the Office of Naval Research, Contract N00014-79-C-0004.

REFERENCES

Brown, R., 1980: A numerical study of radiation fog with an explicit formulation of the microphysics. *Quart. J. Roy. Meteor. Soc.*, **106,** 781–802.

Csanady, G. T., 1973: *Turbulent Diffusion in the Environment.* Reidel, 248 pp.

Dillon, T. M., J. G. Richman, C. G. Hansen and M. D. Pearson, 1981: Near-surface turbulence measurements in a lake. *Nature,* **290,** 390–392.

Donelan, M. A., 1978: Whitecaps and momentum transfer. *Turbulent Fluxes through the Sea Surface, Wave Dynamics and Prediction.* Favre and Hasselmann, Eds., Plenum Press, 273–287.

Hunt, J. C. R., and A. H. Weber, 1979: A Lagrangian statistical analysis of diffusion from a ground-level source in a turbulent boundary layer. *Quart. J. Roy. Meteor. Soc.*, **105,** 423–443.

Johnson, B. D., and R. C. Cooke, 1979: Bubble populations and spectra in coastal waters; a photographic approach. *J. Geophys. Res.*, **84,** 3761–3766.

Kitaigorodski, S. A., M. A. Donelan, J. L. Lumley and E. A. Terray, 1983: Wave-turbulence interactions in the upper ocean. Part II: Statistical characteristics of wave and turbulent components of the random velocity field in the marine surface layer. *J. Phys. Oceanogr.*, **13,** 1988–1999.

Newberger, P. A., and D. R. Caldwell, 1981: Mixing and the bottom nephloid layer. *Mar. Geol.*, **41,** 321–336.

Pasquill, F., 1974: *Atmospheric Diffusion,* 2nd ed. Horwood, Chichester; Wiley and Sons, 429 pp.

Phillips, O. M., 1977: *The Dynamics of the Upper Ocean,* 2nd ed. Cambridge University Press, 336 pp.

Thorpe, S. A., 1982: On the clouds of bubbles formed by breaking wind-waves in deep water, and their role in air–sea gas transfer. *Phil. Trans. Roy. Soc. London,* **A304,** 155–210.

——, 1984a: A model of the turbulent diffusion of bubbles below the sea surface. *J. Phys. Oceanogr.*, **14,** 841–854.

——, 1984b: Bubble clouds: a review of their detection by sonar, of related models, and of how K_v may be determined. *Oceanic Whitecaps and their Role in Air-Sea Exchange Processes.* E. C. Monahan, Ed., Galway University Press (in press).

——, 1984c: The effect of bubbles produced by breaking wind-waves on gas flux across the sea surface. *Ann. Geophys.*, **2,** 53–56.

——, and A. J. Hall, 1983: The characteristics of breaking waves, bubble clouds, and near-surface currents observed using side-scan sonar. *Cont. Shelf Res.*, **1,** 353–384.